TURBOMACHINERY & PUMP SYMPOSIA | HOUSTON, TX
SEPTEMBER 13-15, 2022
SHORT COURSES: SEPTEMBER 12, 2022

ROTORDYNAMIC STABILITY OF A CENTRIFUGAL COMPRESSOR VALIDATED BY MAGNETIC BEARING EXCITER DURING FULL LOAD FULL PRESSURE (FLFP) TESTING

Tingcheng Wu
Senior Rotordynamic R&D Engineer
Siemens-Energy
Houston, Texas, USA

Mark J. Kuzdzal
Past Head, Core Technologies (Retired)
Siemens-Energy
Olean, New York, USA

Dr. Tingcheng Wu is a senior Rotordynamic R&D Engineer at Siemens-Energy. His duties includes torsional and lateral rotor dynamic analysis, bearing and seal design, and machinery vibration analysis. In addition, he has developed several automation tools for the company's in-house rotordynamic analysis. He received his B.S. in mechanical engineering from Nanjing University of Science and Technology in 2011. After that, he worked as a mechanical engineer at China Aerospace Research Academy. He received his M.S. in mechanical engineering from the University of Houston in 2014, and his Ph.D. degree in mechanical engineering from Texas A&M University in 2019. His interests include numerical and experimental analyses of turbomachine rotordynamics and vibration issues. He has published 21 technical papers and reports in international conferences and journals. Dr. Wu is a session chair for the Structures and Dynamics section of the ASME IGTI Turbo Expo Conference, and he also serves as the Technical Editor for STLE Tribology and Lubrication Technology.

Mark Kuzdzal retired from Siemens-Energy (formerly Dresser-Rand) in 2022 with over 34 years of experience in the turbomachinery industry. Mark was most recently the Head of the Core Technologies organization for Siemens-Energy. In this role he had responsibility for Rotordynamics, Materials & Welding, Solid Mechanics, Aero/thermo dynamics and Acoustics disciplines. Mark has also been responsible for guiding development of the advanced compression platform. Mark started his career with Dresser-Rand as a Rotordynamics engineer after earning a B.S. Degree (Mechanical Engineering, 1988) from the State University of New York at Buffalo. Mr. Kuzdzal's areas of expertise focus on rotordynamics, bearing performance, and product/process development. He has co-authored numerous technical papers and holds many patents. Mr. Kuzdzal is an emeritus member of the Texas A&M turbomachinery advisory committee and the Penn State Behrend Mechanical Engineering Technology industrial advisory committee. He is an ASME member.

ABSTRACT

As speed and power density increase, open (unshrouded) impellers are becoming more and more utilized in process gas compressors. Open impellers enable higher tip speeds and more aerodynamic head per stage than closed impellers. However, the industry still lacks maturity and experience of rotordynamic stability assessment with single shaft multistage compressors when open impellers are used. To accurately assess the stability of compressors with open impellers, the estimation of the destabilizing fluid force induced by open impellers is important. The American Petroleum Institute (API) uses the anticipated cross-coupling (Q_A) to estimate the induced rotordynamic destabilizing forces, whereas this empirical Q_A number was initially derived for applications with closed (shrouded) impellers.

This paper presents the measured and predicted stability (log dec.) results from a full-load, full-pressure test with a magnetic bearing exciter of a 6 stage back-to-back centrifugal compressor for natural gas processing. The compressor has three open impellers in the first section, and (three) closed impellers in the second section. The unit was tested to 17,800 RPM with a shaft end horsepower of 20,500 H_P (15.3 MW). The labyrinth seals at interstage and balance piston locations are equipped with swirl brakes to reduce the cross-coupled effects. The magnetic bearing exciter (MBE) test provides the rotor stability results and thus helps to confirm calculated impeller-induced destabilizing forces. The comparison of the impeller-induced destabilizing forces (K_{xy} obtained through different methods, namely, PACC (Predicted Aerodynamic Cross-Coupling), Wachel, CFD (Computational Fluid Dynamics), and measurements, gives

the industry insight into the open impellers and their induced destabilizing forces. This paper provides additional test data in the open literature.

INTRODUCTION

Unshrouded or open impellers have long been used in centrifugal compressors when high head levels or high-pressure ratios are required. They are very common in turbochargers, gas generator sections of gas turbines and integrally geared compressors. Having no shroud or cover, these impellers can operate at higher tip speeds than conventional shrouded or covered impellers due to the lower inherent stresses, i.e., without the cover pulling outward during operation. In some gas turbine or turbocharger applications, unshrouded impellers operate at tip speeds more than 2,000 feet per second (610 meters per second).

One of the most important factors in attaining high aerodynamic performance from unshrouded impellers is the tip clearance between the top of the rotating blades and the adjacent stationary wall or shroud. As the tip clearance increases, the performance of the impeller deteriorates. Further, if the clearance becomes excessively large, it might not be possible to operate the compressor in an aerodynamically stable fashion, not to mention the possible effect on the amount of cross-coupled excitation generated by the impeller.

Unshrouded impellers have historically been used sparingly in beam style multi-stage, single shaft applications. One example of their successful use is in charge gas compressors for ethylene production or similar processes. In all known cases, such compressors included a maximum of two unshrouded impellers in series or at opposite ends of a double-flow rotor. To that end, there is limited information in the literature on lateral rotordynamic stability of beam style centrifugal compressors rotor with open impellers. Albeit focused on shrouded impellers and a unit with oil film seals, an excellent reference paper for lateral rotordynamic stability can be found by Kocur et al.[1].

The authors are aware of two papers in the open literature that capture research and experimental work related to shrouded and open pump (liquid) impellers. It is recognized by the authors that pumps work on an incompressible fluid and compressors work on a compressible fluid, but for the sake of completeness the authors have included the most relevant papers available in the open literature. Uchiumi et al. [2] discussed the design of shrouded and unshrouded liquid fuel rocket turbopump impellers. In this paper rotordynamic fluid forces are reported using water as a medium and an experimental apparatus energized with an active magnetic bearing. The paper indicates the inertia effect becomes large with increasing impeller whirl angular velocity / spinning angular velocity (ω/Ω) for the open impeller and the restoring effect (damping) becomes large for the closed impeller. In addition, the impeller shroud reduces the direct stiffness coefficient and the direct added fluid mass coefficient. Finally, the relationship between direct damping coefficient and added fluid mass cross-coupled coefficient is nearly linear for the open and closed impellers.

The paper from Jolly et al. [3] compares experimental rotordynamic force coefficients produced by both open and shrouded pump impellers in water with a 13.8 inch (350 mm) impeller diameter and water inlet pressure of 86 PSI (0.6 MPa). The test resulting indicates the open impeller produced lower direct stiffness and direct damping coefficients compared to the shrouded impeller, which is fitted with an eye-packing seal. But cross-coupled stiffness and damping coefficients are almost the same for both types of impellers.

Wiesche and Passmann [4] investigated steam turbine blade tip excitation forces via computational fluid dynamics (CFD) and experimental cascade results. Their results indicate the aerodynamic cross-coupling effect decreases as the blade tip gap grows. Through the CFD and experimental data, the authors derived a nonlinear dependency on the normalized mean tip gap clearance. Later, Pan et al. [5] investigated the turbine blade tip clearance excitation forces in an unshrouded turbine using CFD methods. They analyzed the impact of operating conditions on the cross-coupling stiffness generated by the unshrouded blades and found that the cross-coupling effects decreased with respect to an increase in rotor speed. On the other hand, for a small tip clearance (normalized mean tip clearance ~1%), increasing the tip clearance leads to an increase in the cross-coupling effect, while for a large tip clearance (normalized mean tip clearance ~3%), the correlation is opposite. Additionally, the analysis indicates that the effects of inlet flow angle and eccentricity ratio are negligible. All these works have been completed with axial flow turbines, and little information exists for open impellers operated in gas compressors.

The demand for higher pressure ratios in a single compressor has led to a renewed interest in using multiple open impellers in single shaft (beam style) gas compressors. The increased pressure ratio and volume reduction attainable by unshrouded impellers allows more work to be done on the flow with a fewer number of impellers. This also presents a potential risk of creating an unstable rotor system. Moore et al. [6] is one of the earlier papers which addresses how measured rotordynamic stability changes with speed, power and gas density. Using a magnetitic bearing exciter, the authors demonstrated with proper management of flow in the secondary flow passages the rotor can become more stable as speed, power and gas density increase.

This paper describes recent experiences with a compressor developed for a relatively low molecular weight application with a focus on reducing the size of the compression package. To attain the necessary pressure ratio while simultaneously reducing the case size, it was necessary to operate at tip speeds higher than could be tolerated by shrouded impeller designs. Therefore, unshrouded impellers were applied. The authors' company has extensive experience with such impellers in integrally geared arrangements. However, much of that

experience has been in single-stage, overhung configurations. The unit developed was a six-stage back-to-back, single-shaft compressor with three open impellers in series in the first section and three closed impellers in series in the second section.

A full-size prototype of the six-stage compressor was built and subjected to ASME PTC-10 type 2 sectional test to demonstrate that the unit was aerodynamically acceptable. The unit was also tested to demonstrate acceptable rotordynamics per API 617-8th edition. The unit successfully passed the 4 hour no load mechanical test and the 4-hour full-load full-pressure test.

PREDICTION MODEL DEVELOPMENT

Direct measurement of system damping is difficult and not practical in experimental tests. Instead, deriving the system damping from measured vibration data is commonly used in engineering practice. The derivation below demonstrates the relationship between vibration results and system damping.

Assuming an unbalance excitation applied to the rotor system, the equation of motion is generalized as $M\ddot{x} + C\dot{x} + Kx = Me\omega^2 e^{i\omega t}$, where $x = Z \cdot e^{i\omega t}$ and Z is a complex number.

$$-\omega^2 MZe^{i\omega t} + i\omega CZe^{i\omega t} + KZe^{i\omega t} = Me\omega^2 e^{i\omega t} \tag{1}$$

$$\frac{Z}{e} = \frac{M\omega^2}{K - \omega^2 M + iC\omega} = \frac{\omega^2}{\frac{K}{M} - \omega^2 + i\frac{C\omega}{M}} \tag{2}$$

As $\omega_n = \sqrt{\frac{K}{M}}$, $\xi = \frac{C}{2\sqrt{KM}} = \frac{C}{2\omega_n M} \Rightarrow \frac{C}{M} = 2\xi\omega_n$

When system damping is small, then, $\xi^2 \to 0$, and $r = \frac{\omega_{ur}}{\omega_n} = \frac{1}{\sqrt{1-2\xi^2}} \to 1$ (i.e., $\omega_{ur} = \omega_n$). Thus, peak response amplitude is

$$\left|\frac{Z}{e}\right|_{Max} = \frac{r^2}{\sqrt{(1-r^2)^2 + 4\xi^2 r^2}} = \frac{1}{2\xi} \tag{3}$$

At the half-power point per API 617 [7], the amplitude equals to $1/\sqrt{2}$ × Maximum Amplitude

$$\left|\frac{Z}{e}\right|_{Half-Power} = \frac{1}{\sqrt{\left(1 - {r_{1,2}}^2\right)^2 + 4\xi^2 {r_{1,2}}^2}} = \frac{\left|\frac{Z}{e}\right|_{Max}}{\sqrt{2}} = \frac{1}{2\sqrt{2}\xi} \tag{4}$$

Thus,

$$\frac{1}{\sqrt{\left(1 - {r_{1,2}}^2\right)^2 + 4\xi^2 {r_{1,2}}^2}} = \frac{1}{2\sqrt{2}\xi} \tag{5}$$

For small system damping ($\xi < 0.2$, AF >2.5), $\xi^2 \approx 0$, thus,

$$2\xi = \frac{\omega_2 - \omega_1}{\omega_n} \tag{6}$$

Recall the API 617 definition of Amplification Factor (AF), then

$$AF = \frac{\omega_n}{\omega_2 - \omega_1} = \frac{1}{2\xi} \tag{7}$$

In engineering practice, the log dec. (δ) is utilized instead of the damping ratio (ξ) to evaluate the system damping level, where

$$\delta = 2\xi * \pi = \frac{\pi}{AF} \tag{8}$$

Thus, the compressor log dec. can be calculated from the measured vibration amplification factors (AFs).

The compressor along with the Magnetic Bearing Exciter (MBE) is modeled in a 2D rotordynamic analysis package, shown in Figure 1 below. The compressor has two sections separated by a division wall (D Wall). To estimate the compressor log dec. at the operating

speed a harmonic excitation was applied at the thrust end. The anticipated cross-coupling effects from the open impellers are evaluated with different methods and applied to the rotor model. Figure 2 depicts the predicted mid-span unbalance response, which indicates the first critical speed at 6,500 CPM and the second critical speed of 22,500 CPM. Therefore, to measure the system stability at the first critical speed, a frequency sweep from 2,000 CPM to 9,000 CPM is sufficient.

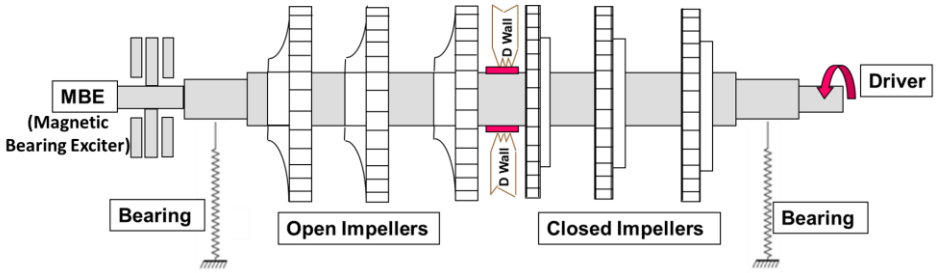

Figure 1. Schematic view of rotor model (not to scale)

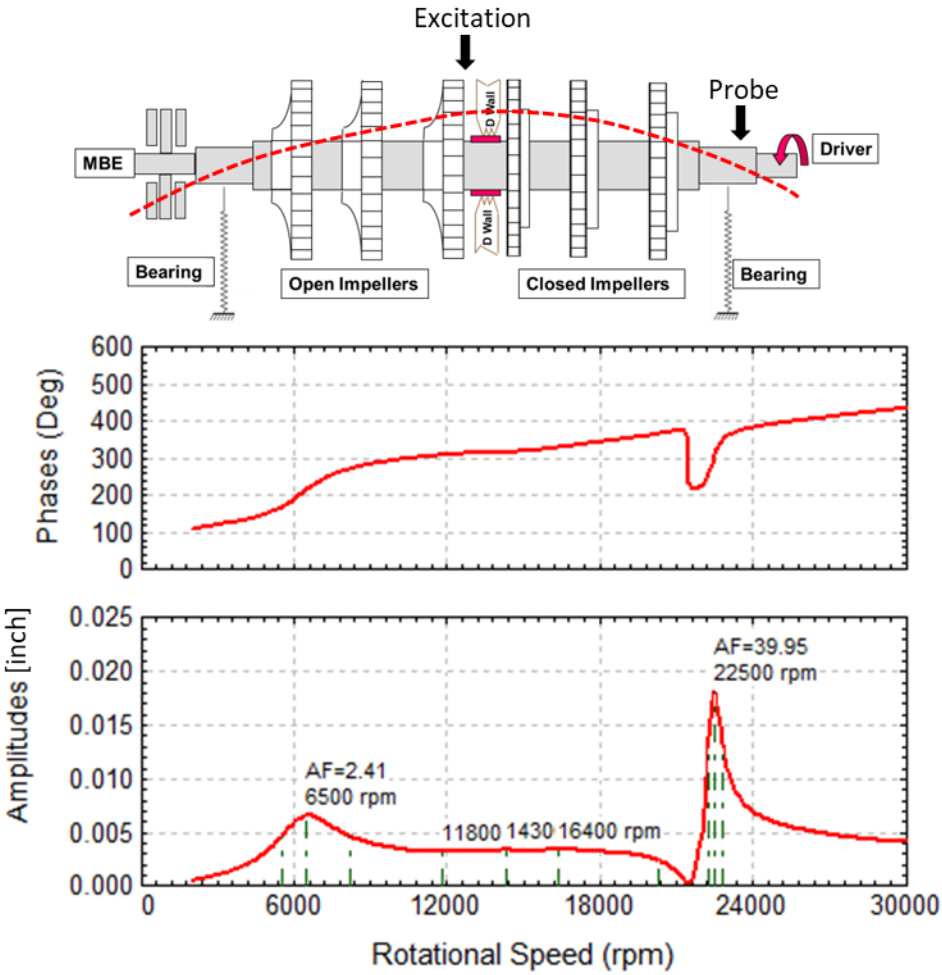

Figure 2. Predicted mid-span unbalance response

PREDICTED ROTOR STABILITY

The aerodynamic excitation caused by the impeller clearance variation acts as a destabilizing force to the rotor system, and the destabilizing force is modeled in terms of the cross-coupling coefficients (K_{xy} and K_{yx}) applied at the rotor mid-span:

$$\begin{bmatrix} F_x \\ F_y \end{bmatrix} = \begin{bmatrix} 0 & K_{xy} \\ K_{yx} & 0 \end{bmatrix} \begin{bmatrix} x \\ y \end{bmatrix} \tag{9}$$

Alford [8] proposed an empirical equation to estimate the cross-coupled stiffness of each stage

$$q_a = K_{xy} = -K_{yx} = \frac{\beta T}{DH} \tag{10}$$

where K_{xy} stands for the aerodynamic excitation, T is the stage torque (lbf-in), D is the blade pitch (mean) diameter (in), H is the blade height (in), and β is the efficiency factor (design factor). Alford's equation was originally developed for axial flow turbines and compressors: Kirk and Donald [9] also use this equation for centrifugal compressors, and commercial software from Texas A&M University recommend the $\beta = 2 - 3$ for unshrouded radial flow impellers [10, 11].

In 1983, Wachel [12] proposed a different formula including the processing fluid properties to estimate the aerodynamic cross-coupled stiffness of each stage:

$$q_a = K_{xy} = -K_{yx} = \frac{6300 H_P M_w}{DHN_r} \frac{\rho_d}{\rho_s} \tag{11}$$

where, H_P is the stage power (horsepower), M_w is the molecular weight, D is the impeller outer diameter (in), H is the blade height (in), N_r is the rotor speed (RPM), ρ_d is the discharge fluid density, and ρ_s is the suction fluid density. The famous Wachel equation encompasses all internal excitations (destabilizing forces) between the case and end seals. Therefore, the Wachel's equation does not represent solely an aerodynamic destabilizing effect due to the impellers vanes, but also includes all other sources such as labyrinth seals, impellers, balance piston, etc. [13].

API 617 eight edition [7] proposes a modified version of the Wachel's equation (Predicted Aerodynamic Cross-Coupling (PACC) number),

$$q_a = PACC = K_{xy} = -K_{yx} = \frac{H_P B_c C}{DHN_r} \frac{\rho_d}{\rho_s} \tag{12}$$

where, $B_c = 3$, and $C = 9.55$ (SI) or 63 (imperial units h) are two constants. Through the many years' practice, the authors company verified and recommended a modified PACC number (MPACC) = 0.8×PACC to better estimate the aerodynamic cross-coupling effect [14].

$$q_a = K_{xy} = -K_{yx} = MPACC = 0.8 \times PACC = 0.8 \times \left\{ \frac{H_P B_c C}{DHN_r} \frac{\rho_d}{\rho_s} \right\} \tag{13}$$

The above formula is for each impeller stage and summing up the coefficients for all stages gives the whole compressor aerodynamic cross-coupling coefficients, $Q = \sum q_a$.

A Computational Fluid Dynamics (CFD) analysis serves to assess the cross-coupling effects created by the open impellers. In the CFD analysis for each open impeller stage, a rotating reference frame method [15] along with eccentricity serves to deliver both the radial and tangential forces induced by the impellers. The authors' prior research [16, 17] proved that 5% of radial clearance motion amplitude is sufficient to generate the reaction forces to extract the coefficients.

$$\begin{cases} \dfrac{F_r}{e} = -K_{XX} - C_{XY}\omega + M_{XX}\omega^2 \\ \dfrac{F_t}{e} = K_{XY} - C_{XX}\omega - M_{XY}\omega^2 \end{cases} \tag{14}$$

where, F_r and F_t are the radial and tangential direction reaction forces obtained by integrating the pressure field on the impeller surface; e = 5%×radial gap; ω is the whirling frequency. K_{XX}, C_{XX}, M_{XX} represent the direct stiffness, damping, and added-mass coefficients, while K_{XY}, C_{XY}, M_{XY} represent the cross-coupled stiffness, damping, and added-mass coefficients from the curve fit of the force impedance (F_r/e, F_t/e) versus the whirling frequency. Therefore, the CFD predicted cross-coupling coefficient Q = 8,467 lbf/in, which is about 44% of the API 617 defined PACC value. Please note that the API value is intended to represent all internal destabilizing forces, whereas the CFD values reported are for the open impellers alone and do not include other internal destabilizing forces.

A magnetic bearing exciter (MBE) was mounted at the thrust end to generate planar excitation force along the 45° direction during the FLFP test. The rotor speed is set as 17,842 RPM to simulate the test condition, and the harmonic excitation frequency ranges from 2,000 CPM to 9,000 CPM. In the prediction model, the aerodynamic cross-coupling coefficient *Q* is applied at the mid-span of the rotor per API 617 8th edition requirement.

As mentioned earlier that the Wachel's model, the API 617 PACC model, and the MPACC model include all the cross-coupling effects from flange to flange, while the CFD method and the Alford's model only apply wheel by wheel [13]. Therefore, to compare those models, it is necessary to include the labyrinth seal effects in the calculations for the CFD and Alford's model, Table 1 lists the labyrinth seals' cross-coupling coefficients for the open impellers (at full-load-full-pressure conditions). Table 2 lists the cross-coupling coefficients applied to the calculation for each model.

To align with the MBE test, the authors applied a harmonic excitation with 250 lbs force (amplitude) on the rotor thrust end (where the MBE mounted) at 17,842 RPM. Figures 3 – 7 illustrate the predicted harmonic excitation responses with these cross-coupling coefficient (*Q)*. Table 2 includes the corresponding log decs (δ) for each model, respectively. Later, these predictions are compared against the test measurements.

Table 1. Predicted interstage labyrinth seal cross-coupling coefficients for the open impellers at full load conditions

	Laby-1	Laby-2	Laby-3	Balance Piston
Cross-coupling Coefficient [lbf/in]	1,216	1,136	914	2,198

Table 2. Predicted aerodynamic cross-coupling coefficients *Q* and Amplification Factors (AFs) at full load

Method	**API 617 PACC**	**MPACC**	**Wachel's Model**	**Alford's Model + Labys**	**CFD+ Labys (for open Impellers section)+PACC(closed impellers)**
Cross-coupling Coefficient *Q* [lbf/in]	**19,440**	**15,552**	**32,914**	**31,484**	**13,941**
Predicted AF of NC1 (first natural frequency)	8.04	7.1	18.14	16.84	6.84
Predicted log dec (δ)	0.39	0.44	0.17	0.19	0.46

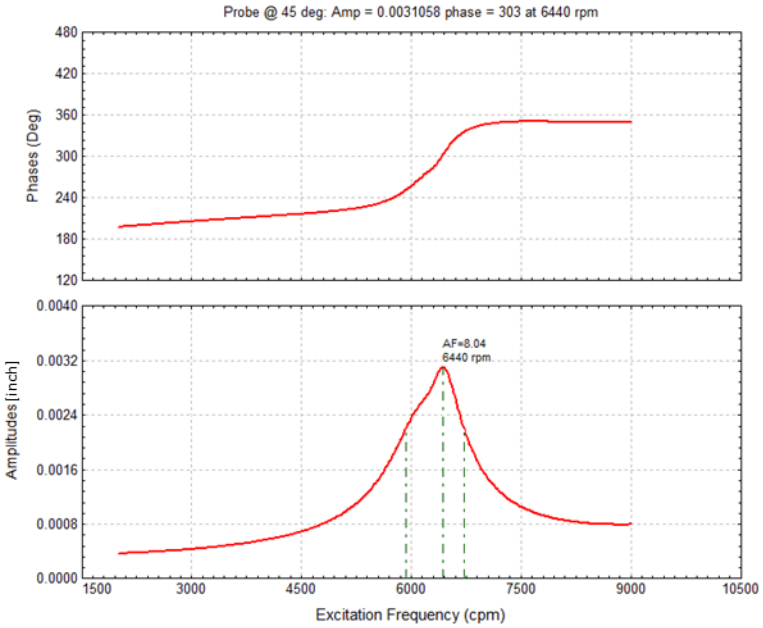

Figure 3. Predicted harmonic excitation response with API 617 PACC model *Q* =19,440 lbf/in

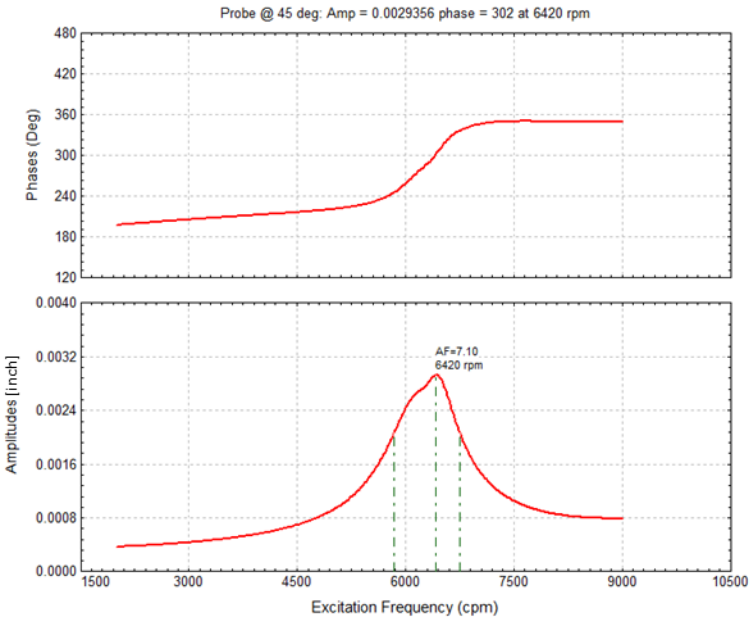

Figure 4. Predicted harmonic excitation response with MPACC model *Q* =15,552 lbf/in

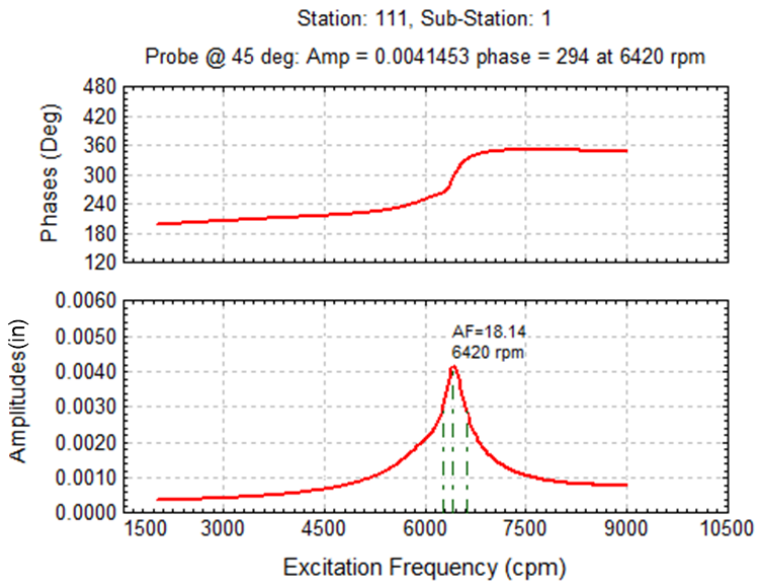

Figure 5. Predicted harmonic excitation response with Wachel's model *Q* = 32,914 lbf/in

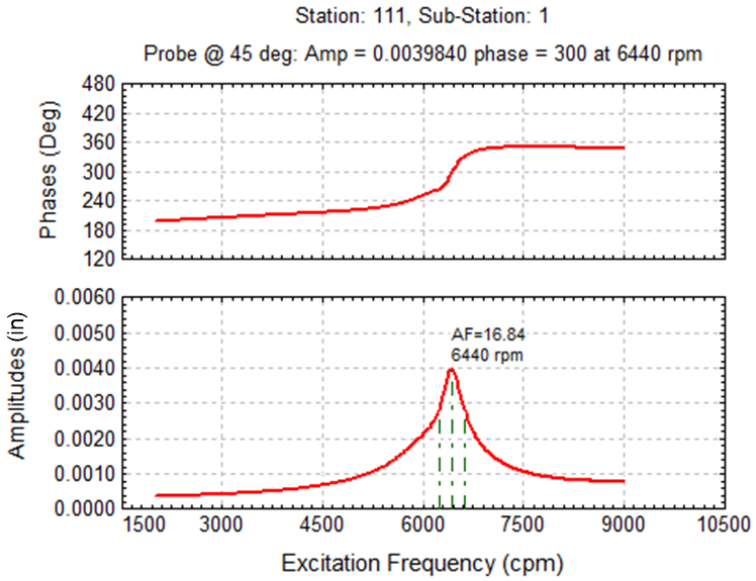

Figure 6. Predicted harmonic excitation response with Alford's model *Q* + labyrinth seal =31,484 lbf/in

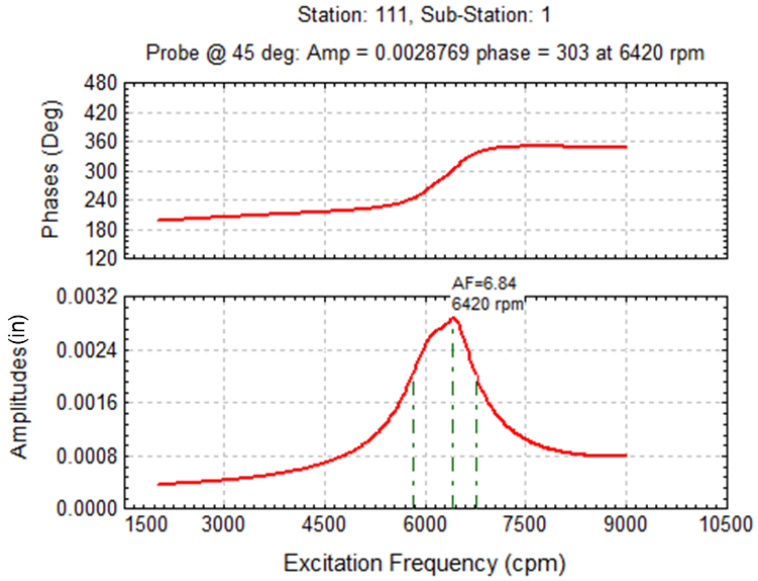

Figure 7. Predicted harmonic excitation response with CFD derived *Q* + labyrinth seal for open impeller section and PACC for the closed impeller section =13,941 lbf/in

INTRODUCTION OF TEST HARDWARE AND SET-UP

The scope of this program included engineering, manufacturing, assembling, and testing a full-size prototype. The unit tested has 125 mm (4.92 inch) five shoe tilt pad journal bearings, 135 mm (5.31 inch) tandem dry gas seals, 305 mm (12.0 inch) self-leveling thrust bearings. Additionally, the unit has ~ 470 mm (18.5 inch) impeller diameters and a 1.46 meter (57.5 inch) bearing span. The shaft power is 15.39 MW (20,500 H_P). An OEM owned turbine along with a parallel axis gear (gear ratio of 3.13) serves to drive the compressor. To satisfy the customer requirement for acid wash, the rotor construction included 15-5 martensitic precipitation-hardening stainless steel (see Figure 8).

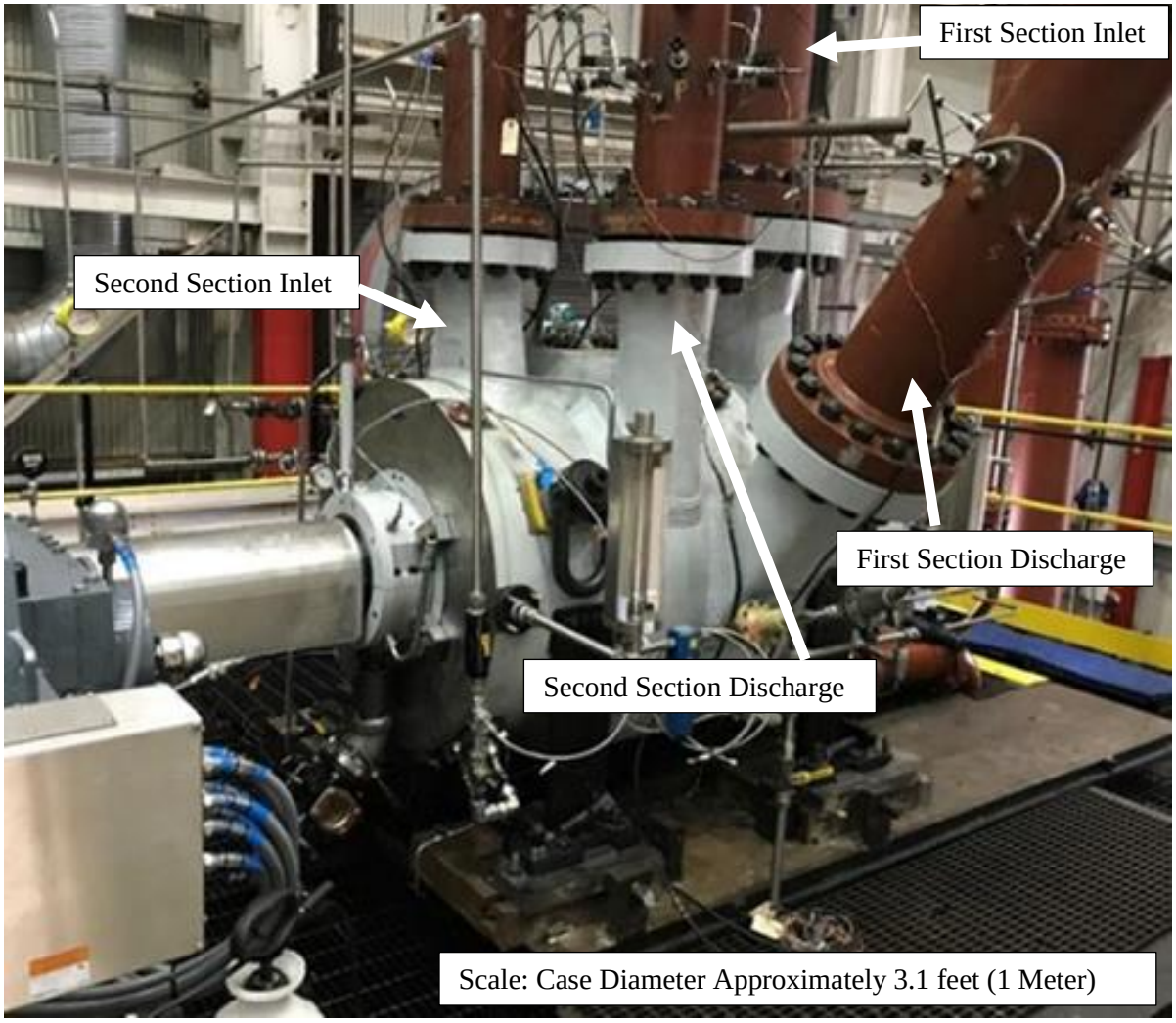

Figure 8. Full size prototype on test bed

As discussed earlier, the back-to-back compressor included a 6-stage (3+3) rotor using three open (unshrouded[1]) impellers in the first section. See figures 9 and 10. This was the first time in the authors experience where three open impellers were utilized in succession. The first process section is the low-pressure stage and is located on the service side of the compressors.

To control impeller tip gap clearance and preserve aerodynamic efficiency, the open impellers employ a stationary contour ring with an abradable coating. These three contour rings were rail fit into the diaphragm and shimmed at assembly to avoid rubbing but maintain a tight clearance. At start-up the rotor will heat up faster than the stator, the compressor configuration allows the open impellers to grow away from, rather than into, the contour rings during transient periods. The back-to-back unit was driven from the second section discharge with the thrust bearing on the inlet end of the machine. Starting cold, as the rotor comes to speed, it will warm faster than the corresponding stationary components. With the thrust bearing on the inlet side as close as possible to the open impellers the rotor will grow away for the stationary contour rings. The compressor feet are anchored to the base plate at the inlet end. As the unit reached thermal steady state, the impeller's tip gap close to a predetermine magnitude. Using a hot-to-cold axial growth conversion, the contour rings were shimmed at assembly to a specific value.

[1] The impellers have full diameter disk, which is also called semi-open in the literature.

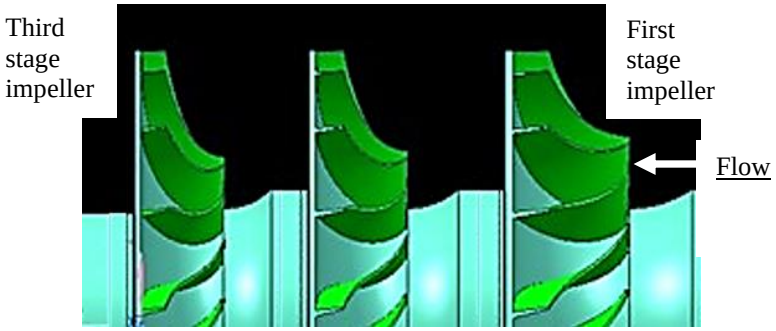

Figure 9. Three open impellers in series

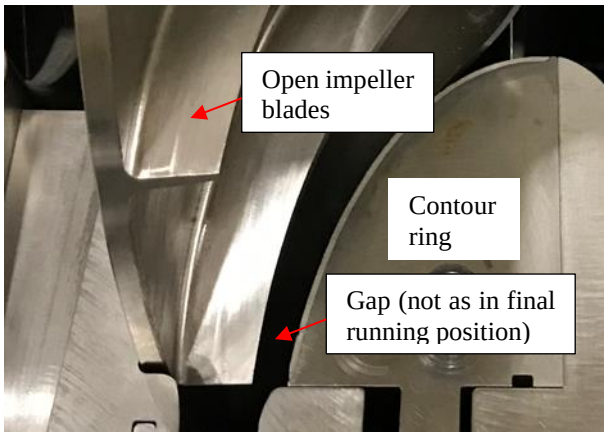

Figure 10. Unshrouded (open) impeller with contour ring (*rotor & contour ring not in final running position*)

Throughout the testing, vibrations were monitored for signs of rubbing. None were detected. Post-test inspection also showed that no rubbing had occurred. The second section of this back-to-back unit utilized conventional shrouded impellers.

The magnetic bearing exciter (Figure 11) was mounted outboard of the thrust bearing on the non-drive end of the compressor (closest to the first section, see Figure 12). The system utilized was manufactured by one of the major magnetic bearing companies and could be operated under two excitation modes, namely, internal excitation and external excitation. The internal excitation method uses the signal generator integrated in the system controller to generate either forward or backward rotor whirl excitations. On the other hand, the external excitation method requires an external signal generator to provide excitations. However, one should note that the external excitation method can only generate planar excitation. During the test, the internal signal generator was found not capable to generate sufficient excitations. Thus, the planar excitation method with an external signal generator was selected.

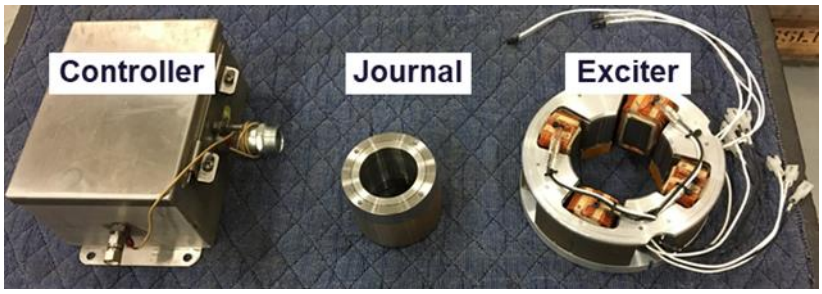

Figure 11. Magnetic bearing exciter (MBE) system

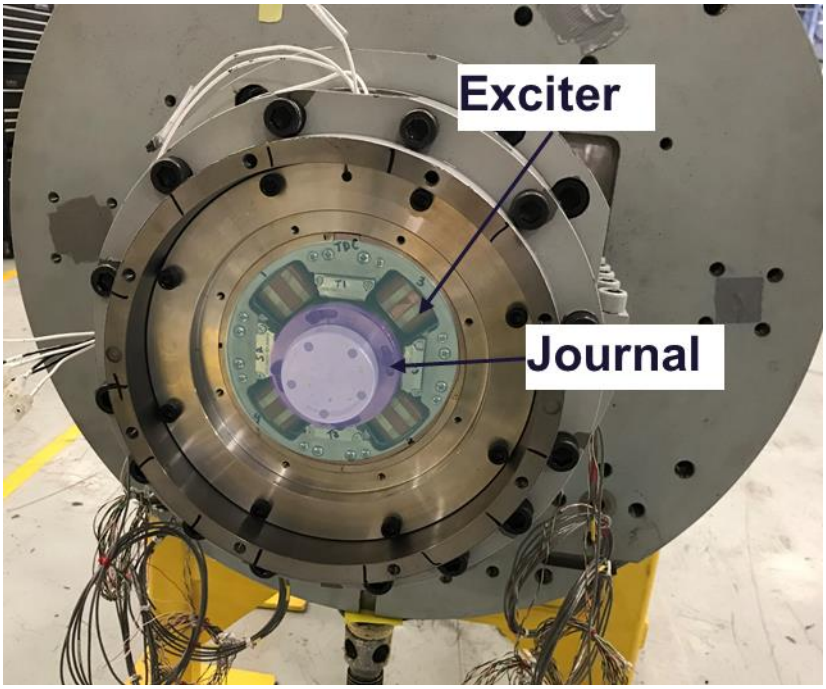

Figure 12. MBE mounted on the compressor shaft end

The magnetic bearing exciter tests were conducted under light load, half load, and full load conditions. The magnetitic bearing was capable of producing 250 lbf (1.1kN) force along the 45-degree direction on to the shaft. The rotor's first and second critical speeds were evaluated, and for each critical speed, the forward and backward modes are separated using the in-house developed post-processing tool in Wu and Maier [18].

FULL LOAD FULL PRESSURE TEST RESULTS

The frequency sweeps around the predicted 1st and 2nd natural frequencies serve to identify their locations.. Figure 13 (a) and (b) shows the measured vibration. Please note that due to the control system of the MBE system, the frequency resolution (step) for the 1st mode range is larger, and thus, the measured data has slightly lower fidelity when compared to that for the 2nd mode. The data indicates the rotor NC1 is around 6,500 CPM, and the difference between (due to gyroscopic effect) the 1st forward and backward frequencies are small. Therefore, only one peak is measured in the test. On the other hand, when the speed increases, the impact of the gyroscopic effect increases, leading to a difference between the second forward and backward modes. As depicted in Figure 13 (b), the two distinct peaks around the predicted 2nd mode represent the 2nd forward (23,553 CPM) and backward (21,845 CPM) modes, respectively. The measured vibration amplitude data around the 1st natural frequency shows a higher noise level, therefore, when post-processing the test results, the authors choose to use the phase slope method to give better results [19].

Figure 14 (a) (b) and (c) demonstrate the test measured 1st natural frequency at various compressor load conditions: light load, half-load, and full load. The results indicate the rotor NC1 is around 6,500 CPM for all cases, and the measured log dec. increases with respect to the load condition, as shown in Figure 15 (solid purple line). The dotted line in Figure 15 is the predicted log dec using API methods. Table 3 provides a summary of predicted and measured log dec along with % difference, where positive percentage is under predicting and negative is overpredicting.

At the full load condition, the measurement derived log dec. is 0.45. The MPACC method and the first section CFD + first section labys + second section PACC method show the best agreement with the measured data. The result of Wachel's model has the worst agreement. Utilizing the PACC number equation per API 617, the cross-coupling effect should increase with compressor load, which is counter to the measurements demonstrated in this work (Figure 15). The authors' company has experience and test data from various units that show, with proper management of gas flow in the secondary flow passages, the compressor will become more stable as speed, power, and gas density increase [6].

Table 3. Predicted aerodynamic log dec, measured log dec and % difference (at Full Load Full Pressure condition)

Method	API 617 PACC	MPACC	Wachel's Model	Alford's Model + Labys	CFD+ Labys (for open Impellers section)+PACC(closed impellers)
Measured log dec (δ)	0.45	0.45	0.45	0.45	0.45
Predicted log dec (δ) (from Table 2)	0.39	0.44	0.17	0.19	0.46
Percent difference	13%	2%	62%	58%	-2%

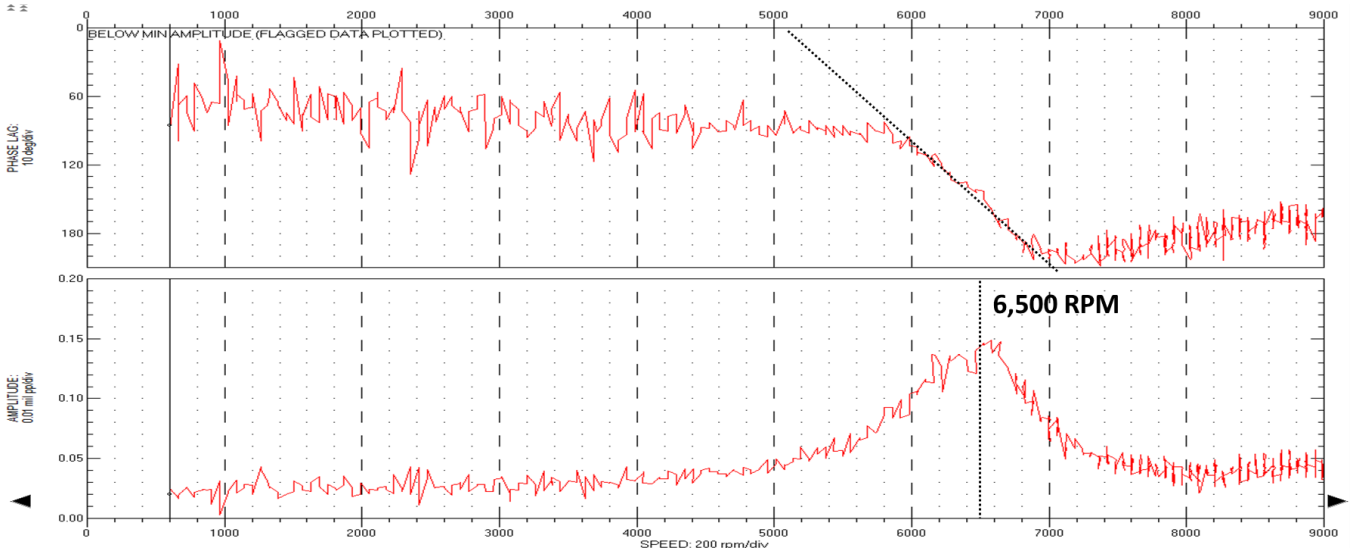

Figure 13 (a). NC1 at full load conditions, drive end Y probe

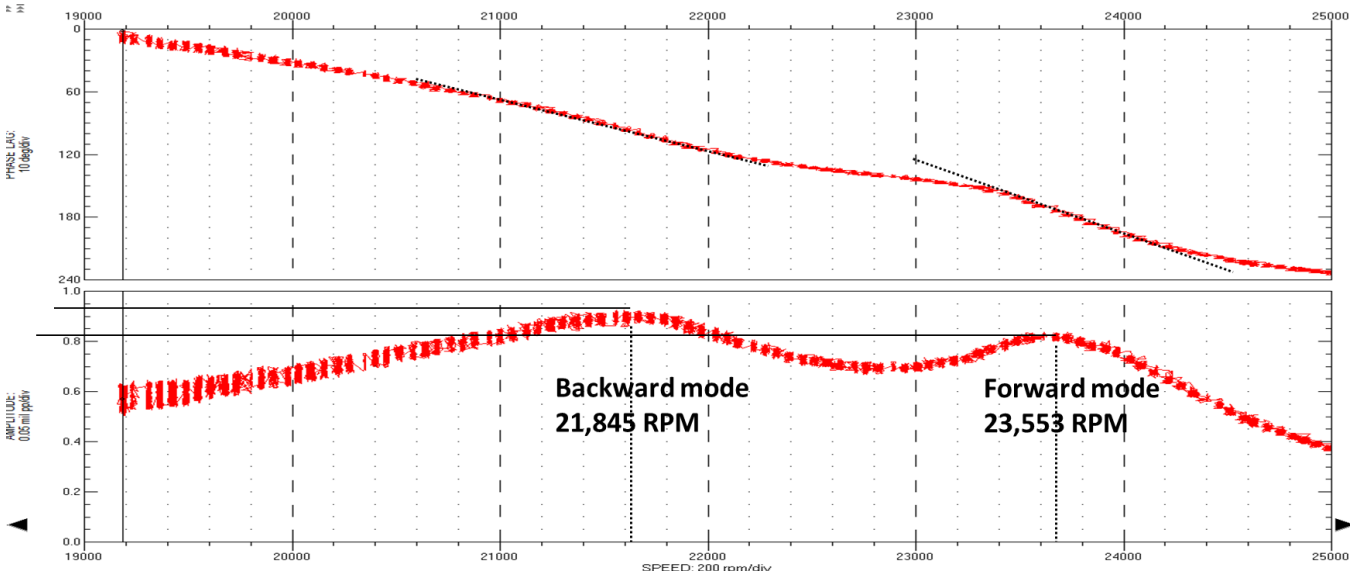

Figure 13 (b). NC2 at full load condition, drive end Y probe

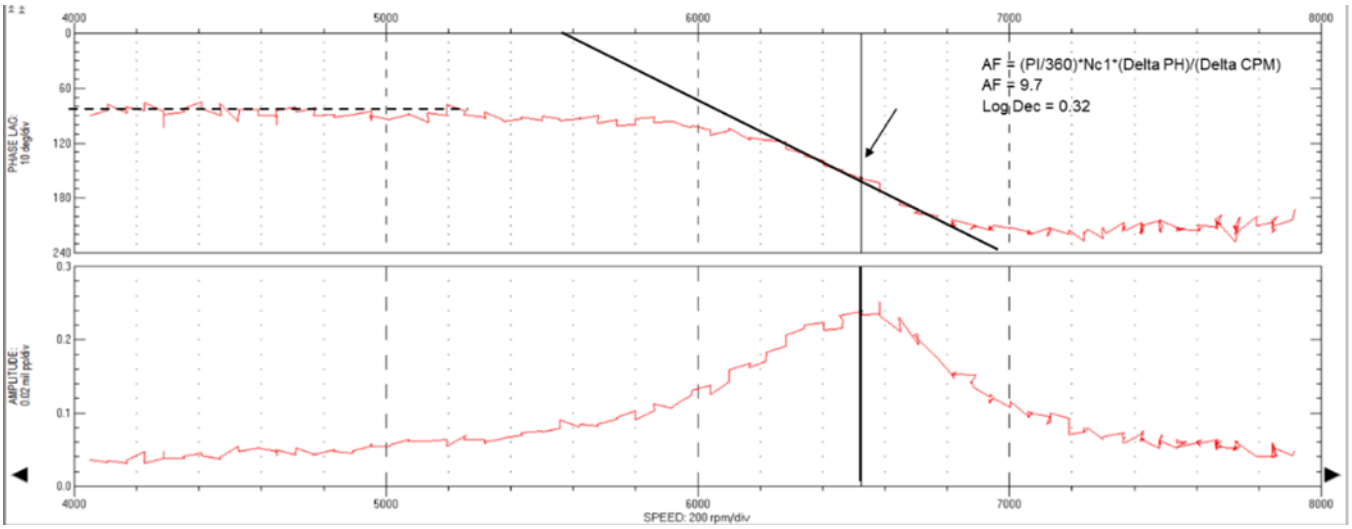

Figure 14 (a). Compressor operated at light load (~ 1,000 HP), drive end Y probe.

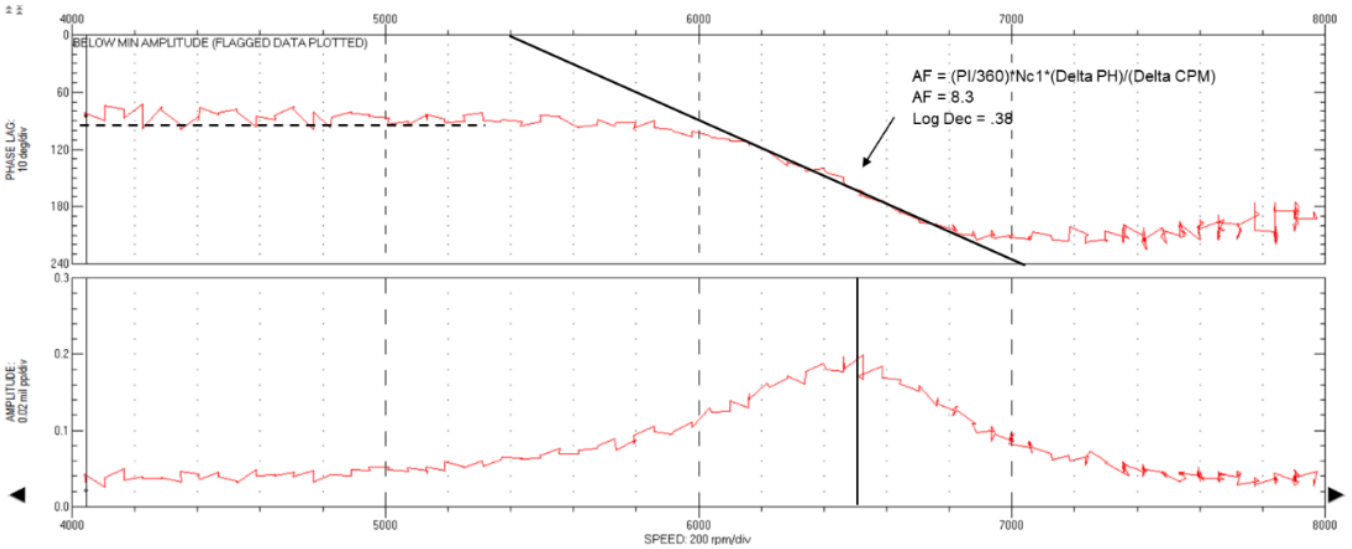

Figure 14 (b). Compressor operated at half load (~ 10,400 HP)at half load, drive end Y probe.

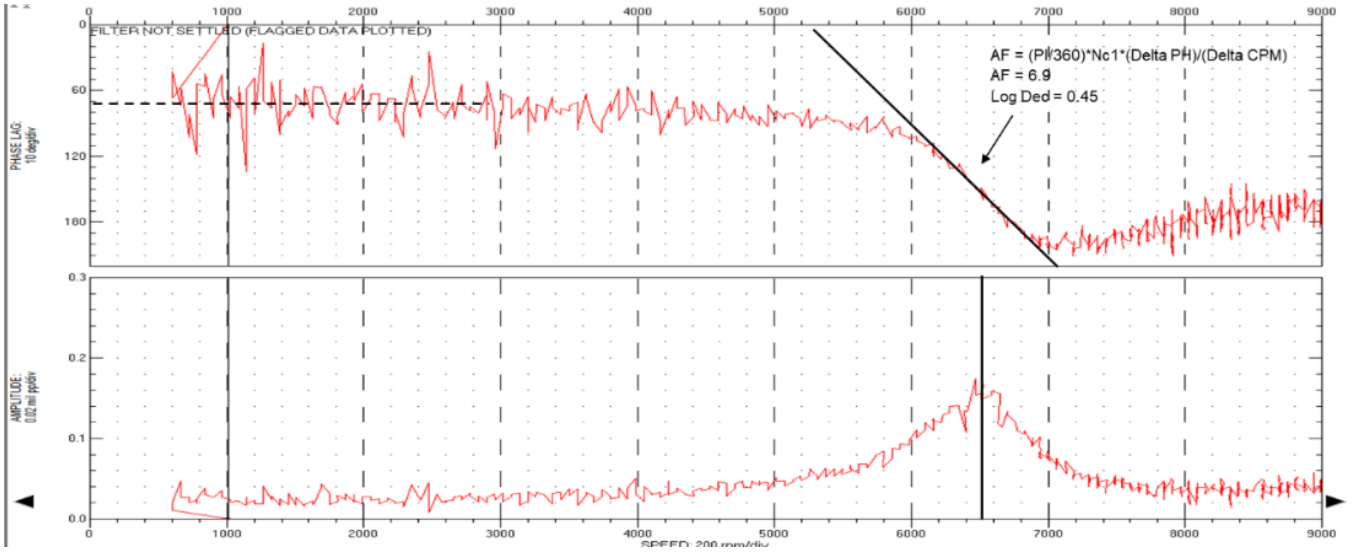

Figure 14 (c). Measured 1st Critical speed vs. compressor full load condition, drive end Y probe.

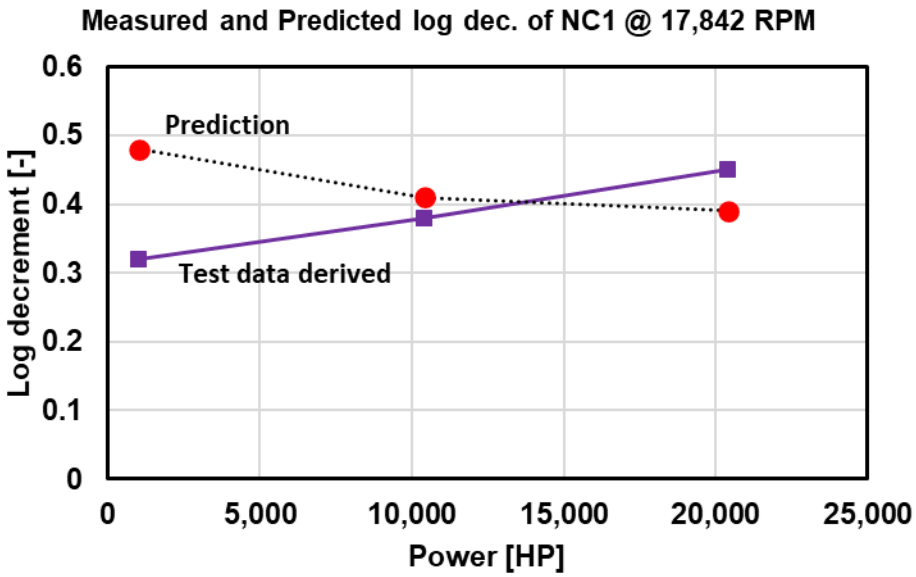

Figure 15. Test derived (solid line) and predicted (dotted line) system log dec. @1st Critical speed vs. compressor load condition (compressor speed at 17,842 RPM)

CONCLUSIONS

This paper discussed prediction and test validation of rotordynamic stability of a beam style centrifugal compressor. The compressor had three open impellers in the first section, three closed impellers in the second section. A magnetic bearing exciter (MBE) was utilized to provide external perturbations to the rotor and extract measured stability results; thus, helping to confirm calculated impeller-induced destabilizing forces. The compressor had labyrinth seals at the interstage and balance piston locations with swirl brakes to reduce the cross-coupled effects.

The unit was tested to 17,800 RPM with a shaft end horsepower of 20,500 H_P (15.3 MW). To accurately assess the stability of compressors with open impellers, various techniques for estimating the destabilizing fluid force induced by said open impellers was explored and presented. The intent was to give the industry more insights into the open impellers, and variation in the prediction of the induced destabilizing forces. Next the paper presents the predicted rotor stability (log dec.) and compares predicted results to full-load, full-pressure magnetic bearing exciter test results. The full load as tested data derived log dec was 0.45, whereas the CFD method predicted 0.46 and the MPACC method predicted 0.44; both methods showing only 2% difference with the test derived result. The other

three different hand calculations methods predict values between 0.17 and 0.39. Considering the complexity of extracting cross-coupling coefficients via CFD simulations, the PACC and MPACC methods provide a reliable with a relatively good accuracy estimate the impeller's aerodynamic induced cross-coupling effect. It is recognized that there are system level influences and the tests do not isolate the open impeller cross coupling from the system. This paper intends to provide additional test data in the open literature.

NOMENCLATURE

AF	Amplification Factor
C	Damping coefficient [Ns/m]
CFD	Computational Fluid Dynamics
C_{XX}, C_{XY}	Direct and cross-coupling damping [N-s/m]
C_{eff}	Effective damping, $C_{eff} = C_{xx} - K_{xy}/\omega$ [N-s/m]
D	Blade pitch (mean) diameter [in]
Di/D2	Hub-to-tip ratio
Di	Minimum diameter of impeller hub aerodynamic flow path
D2	Impeller exit diameter
e	Eccentricity [m]
FLFP	Full-Load-Full-Pressure test
F_r, F_t	The radial and tangential direction reaction forces
f_x, F_x	Horizontal direction reaction force [N]
f_y, F_y	Vertical direction reaction force [N]
H	Blade height [in]
H_P	Stage power (horsepower),
i	Imaginary part
K	Stiffness coefficient [N/m]
KBI	Knowledge Based Impeller
K_{XX}, K_{XY}	Direct and cross-coupled stiffness [N/m]
M	Added mass coefficient[kg]
MBE	Magnetic bearing exciter
MPACC	Modified PACC number, MPACC = 0.8×PACC
Mu2	Machine Mach number (tip speed of impeller related to speed of sound at stage inlet)
M_{XY}, M_{XY}	Direct and cross-coupled added mass [kg]
M_w	Molecular weight
MW	Megawatt
NC1, NC2	1st and 2nd natural frequencies.
N_r	Rotor speed (RPM)
PACC	API 617 defined Predicted Aerodynamic cross-coupled Coefficient.
Q	Total aerodynamic induced cross-coupling effect $Q = \sum q_a$ [lbf/in].
q_a	Anticipated cross-coupled stiffness of each impeller [lbf/in]
r	Frequency ratio $r = \frac{\omega}{\omega_n}$
T	Stage torque [lbf-in],
t	Time [s]
x, y	Displacement along the x and y directions [m]
$\dot{x}$	Velocity along X direction [m/s]
$\ddot{x}$	Acceleration along X direction [m/s^2]
Z	Complex number $x = Z\, e^{\,iwt}$
β	Efficiency factor (design factor).
δ	System log dec.
ξ	Damping ratio
ρ_d	Discharge fluid density [lbm/in^3]
ρ_s	Suction fluid density [lbm/in^3]
ω	Angular velocity [rad/s]
ω_n	Natural frequency [rad/s]
ω_{ur}	Unbalance response frequency [rad/s]

ACKNOWLEDGEMENTS

The authors acknowledge the support of their colleagues in Duisburg, Germany and Olean, N.Y., USA in contributing to the success of this development and test effort. The authors also thank Siemens-Energy for allowing us to publish this paper and the Texas A&M

Turbomachinery Laboratory for providing the excellent venue to present our work.

REFERENCES

[1] Kocur, J., Cloud, C. H., and Pettinato, B., 2018, "Predicting, Understanding and Avoiding the Ekofisk Rotor Instability Forty Years Later," Proceedings of the 47th Turbomachinery Symposium, Houston, Texas., doi:hdl.handle.net/1969.1/174995.
[2] Uchiumi, M., Nagao, N., Yoshida, Y., and Eguchi, M., 2012, "Comparison of Rotordynamic Fluid Forces between Closed Impeller and Open Impeller," Fluids Engineering Division Summer Meeting, **44755**, pp. 521-527, doi: 510.1115/FEDSM2012-72348.
[3] Jolly, P., Bonneau, O., and Arghir, M., 2021, "Rotordynamic Force Coefficients for Open and Shrouded Impellers," Vibration Engineering for a Sustainable Future, Springer, pp. 107-113.
[4] Wiesche, S. a. d., and Passmann, M., "Analysis of Steam Turbine Blade Tip Excitation Forces by Means of Computational Fluid Dynamics and Experimental Cascade Results," Proc. Turbo Expo: Power for Land, Sea, and Air, American Society of Mechanical Engineers, p. V008T029A005, doi:10.1115/GT2018-75179.
[5] Pan, Y., Yuan, Q., Huang, G., Gu, J., Li, P., and Zhu, G., 2020, "Numerical Investigations on the Blade Tip Clearance Excitation Forces in an Unshrouded Turbine," Applied Sciences, **10**(4), p. 1532, doi:10.3390/app10041532.
[6] Moore, J. J., Walker, S. T., and Kuzdzal, M. J., 2002, "Rotordynamic Stability Measurement During Full-Load, Full-Pressure Testing of a 6000 Psi Reinjection Centrifugal Compressor," Proceedings of the 31st Turbomachinery Symposium, Houston, Texas, pp. 29-38., doi:10.21423/R10D3J.
[7] American Petroleum Institute, 2014, "API 617 Standard 8th Edition: Axial and Centrifugal Compressors and Expander-Compressors".
[8] Alford, J., 1965, "Protecting Turbomachinery from Self-Excited Rotor Whirl," ASME J Eng Power, **87**(4), pp. 333-343, doi:10.1115/1.3678270.
[9] Kirk, R., and Donald, G., 1983, "Design Criteria for Improved Stability of Centrifugal Compressors," Proceedings of ASME Applied Mechanics Division (AMD): Rotor Dynamical Instability, **55**, pp. 59-71.
[10] Chen, W., 2021, "Dyrobes User Manual," https://dyrobes.com/help1800/Rotor/html/dyro7iur.htm, accessed on June 29, 2022.
[11] XLTRC2, 2020, "Xltrc2 Software User Manual."
[12] Wachel, J. C., 1983, "Compressor Case Histories, Presented at Rotating Machinery and Controls (Romac) Short Course," University of Virginia, June 8-10.
[13] Evans, B. F., and Fulton, J. W., 2010, "Wachel's Equation-Origin and Current Evaluation of Api 617 Rotor Stability Screening Criteria," Proceedings of the 39th Turbomachinery Symposium, Houston, Texas, pp. 9-18., doi:10.21423/R15932.
[14] Memmott, E., 2000, "Empirical Estimation of a Load Related Cross-Coupled Stiffness and the Lateral Stability of Centrifugal Compressors," CMVA, Proceedings of the Eighteenth Machinery Dynamics Seminar, Halifax, April 26-28, pp. 9-20.
[15] San Andrés, L., Wu, T., Maeda, H., and Ono, T., 2018, "A Computational Fluid Dynamics Modified Bulk-Flow Analysis for Circumferentially Shallow Grooved Liquid Seals," ASME J Eng Gas Turb Power, **140**(1), pp. 0125041- 0125049, doi:10.1115/1.4037614.
[16] Wu, T., and San Andrés, L., 2019, "Gas Labyrinth Seals: On the Effect of Clearance and Operating Conditions on Wall Friction Factors – a Cfd Investigation," Tribol Int, **131**, pp. 363-376, doi:10.1016/j.triboint.2018.10.046.
[17] Wu, T., and San Andrés, L., 2018, "Leakage and Dynamic Force Coefficients for Two Labyrinth Gas Seals: Teeth-on-Stator and Interlocking Teeth Configurations. A Computational Fluid Dynamics Approach to Their Performance," ASME J Eng Gas Turb Power, **141**(4), doi:10.1115/1.4041123.
[18] Wu, T., and Maier, M. D., 2021, "A Novel Method to Separate the Forward and Backward Modes in Turbomachine Tests," Proceedings of the 50th Turbomachinery Symposium, Houston, Texas.
[19] Kocur, J., and Cloud, C. H., 2016, "Shop Rotordynamic Testing--Options, Objectives, Benefits and Practices," Proceedings of the 1st Asia Turbomachinery Symposia, Singapore, pp. 1-23., doi:10.21423/R1B12G.

